

Supplementary Figure legends

Supplementary figure 1: Validation of upregulated expression of KDM2A in plaque. (A) Differentially expressed regulons identified between atherosclerotic plaque and macroscopically intact tissue samples in GSE43292 ($P_{adj} < 0.05$ and $|\text{Fold change}| > 2$). (B) Heatmap showing the top 10 activated and deactivated transcriptional regulators (TRs) in the plaque group. (C) Network displaying three master regulons and their target genes (red line: positive correlation; blue line: negative correlation). (D) Boxplots together with group mean \pm SE illustrating the activities of the three TRs (DLX2, HESX1, and KDM2A) that were up- or down-regulated in the plaque group based on the combine dataset ($n = 235$ in total, AS=195, normal=40). (E) Transcriptional expression of the three TRs (DLX2, HESX1, and KDM2A) between early ($n=13$) and advanced ($n=16$) atherosclerotic plaque groups in GSE28829. Correlation analysis of coronary artery disease (CAD) class with (F) DLX2 and (G) HESX1 in GSE90074. (H) The difference of the three TRs (DLX2, HESX1, and KDM2A) levels between the non-obstructive ($n=50$) and obstructive ($n=93$) CAD groups. (I) Binary regression analysis shows the significant correlation between KDM2A levels and obstructive CAD, adjusting for demographic characteristics (age, sex, diabetes, hypertension, and hyperlipidemia). (J) Enrichment analysis of KDM2A target genes. Correlation analysis was performed using the Spearman's test; for comparisons two groups, data were assessed by Wilcoxon signed-rank test: ns: $P > 0.05$, $*P \leq 0.05$, $**P < 0.01$. Expressions were presented in boxplots together with the group mean \pm SE.

Supplementary figure 2: Inference of immune infiltration revealed the association of KDM2A with macrophage subtypes. (A) Correlation of the three TRs (HESX1, DLX2, and KDM2A) with 28 immune cell types by single sample gene set enrichment analysis (ssGSEA) in the combine dataset. (B) Boxplots show the differences in the proportions of different macrophage subtypes between macroscopically intact ($n=40$) and atheroma plaque tissue ($n=195$) groups based on the combine dataset. (C) The correlation of the three TRs (HESX1, DLX2, and KDM2A) with different macrophage subtypes through four different algorithms (ssGSEA, CIBERSORT, MCP-counter, and xCell) in the combine dataset. Boxplots show the differences in the proportions of different T cell subtypes between macroscopically intact and atheroma plaque tissue group based on (D) GSE43292 and (E) combine dataset. Correlation of the three TRs (HESX1, DLX2, and KDM2A) with different T cell subtypes using four different algorithms (ssGSEA, CIBERSORT, MCP-counter, and xCell) in (F) GSE43292 and (G) combine dataset. Correlation analysis was examined by Spearman's test; for two groups, data were compared by Wilcoxon signed-rank test: $*P < 0.05$, $**P < 0.01$, $***P < 0.001$, $****P < 0.0001$. Expressions were presented as boxplots together with the group mean \pm SE.

Supplementary figure 3: KDM2A exhibits a higher specificity in macrophages. (A) Analysis of the relative expression of KDM2A across various organs based on the data from the GTEx database shown as box/violin plots. (B) t-SNE clustering plots showing a 19 color-coded cell clusters between proximal adjacent (PA) and paired

atherosclerotic core (AC) regions from 3 patient carotid arteries in GSE159677. (C) Violin plot showcasing the top marker genes across all cell types along with their respective cell proportions. (D) Examination of the relative expression levels of KDM2A across different main cell types shown as box/violin plots, as determined by data from the GSE159677 dataset. Data were statistically compared using the Wilcoxon signed-rank test.

Supplementary figure 4: Involvement of KDM2A in macrophage state alterations using single-cell RNA-seq data. (A) Violin plot displaying the expression levels of top marker genes in macrophage subtypes. (B) Bar chart showing the relative frequencies of macrophage subtypes in proximal adjacent (PA) and paired atherosclerotic core (AC) groups. Single-cell trajectories of the macrophages represented through (C) pseudotime, (D) different cell types, (E) different states, and (F) PA and AC groups as analyzed by Monocle. (G) Bar chart showing the relative frequency of macrophage states in PA and AC groups. (H) The difference in KDM2A activity observed across different macrophage states shown as box/violin plots. Data were presented with group mean \pm SE and compared by Wilcoxon signed-rank test. (I) Heatmap showing the expression of inflammatory macrophage and neutrophil markers across different macrophage subtypes. (J) Immunofluorescence illustrating the cells expressing KDM2A co-expressed with Ly6G within the mouse plaque lesions.

Supplementary figure 5: Validation of KDM2A's involvement in macrophage phenotypic transition using Smart-seq2 based scRNA-seq data (GSE260657). t-SNE clustering plots showing a (A) 10 cell populations (a total of 7,686 individual cells), (B) 12 cell clusters, and (C) two groups (asymptomatic and symptomatic groups). (D) Violin plot showcasing the top marker genes across all cell types. (E) Examination of the relative expression levels of KDM2A across different main cell types shown as violin plots. (F) Cluster tree of myeloid cells sub-clustering according to the different resolutions. t-SNE clustering plots showing a (G) 4 cell populations (a total of 2,900 individual cells), (H) 4 cell clusters, and (I) two groups. (I) Heatmap showing the expression of myeloid subtype markers across different clusters. (K) Examination of the relative expression levels of KDM2A across different myeloid subtypes shown as violin plots. (L) Displayed genes ordered by correlation coefficient with KDM2A activity.

Supplementary figure 6: KDM2A is specifically upregulated in ox-LDL treated macrophages. Western blot assays assessing the expression of KDM2A in human umbilical vein endothelial cells (HUVECs) cultured with (A) different concentrations of ox-LDL ($n = 3$ per group) and (B) at different time points ($n = 6$ per group). (C) Similarly, Western blot assay showing the expression of KDM2A in mouse vascular smooth muscle cells (VSMCs) cultured with different concentrations of ox-LDL ($n = 3$ per group). (D) Expressions of KDM2A were examined in bone marrow-derived macrophages (BMDMs) cultured with varying concentrations of ox-LDL ($n = 3$ per group). Changes in KDM2A expression in BMDMs cultured at different time points

were assessed at (E) protein levels (n = 6 per group) and (F) RNA (n = 3 per group). (G) KDM2A expression levels after treatment with three different KDM2A siRNAs (n = 3 per group). (H) Upregulation of potential KDM2A target genes rescued by si-KDM2A (n = 3 per group). Expressions were plotted as bar plots together with group mean \pm SEM. Data were compared by Mann–Whitney U-test for two groups and one-way ANOVA test for more than two groups.

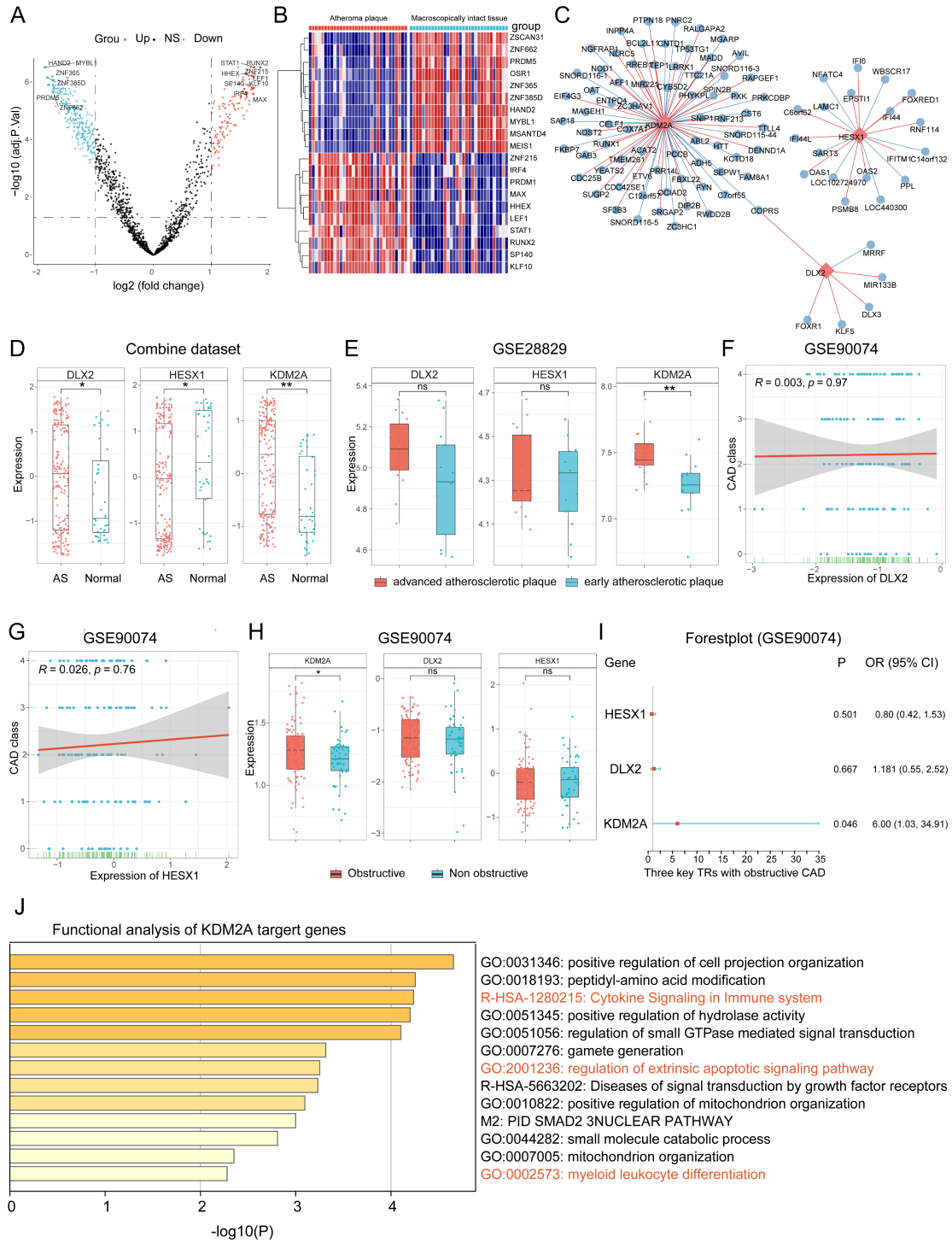
Supplementary figure 7: Correlation analysis of KDM2A with target genes. (A) Gene ontology (GO) analysis of KDM2A binding peaks is presented as a bar chart. Association analysis of KDM2A with (B) FYN and (C) RREB1 using the combine dataset (plaque group, n=195). The association of KDM2A with (D) FYN and (E) RREB1 expression was examined in the GTEx database. Correlation analysis was performed using Pearson test.

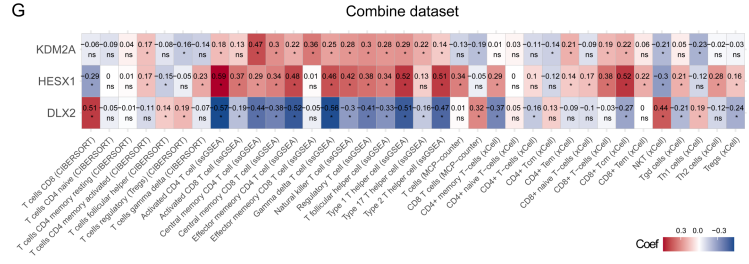
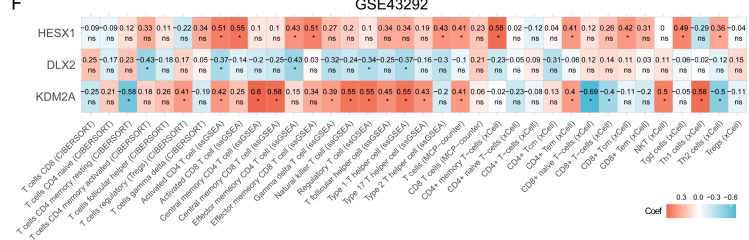
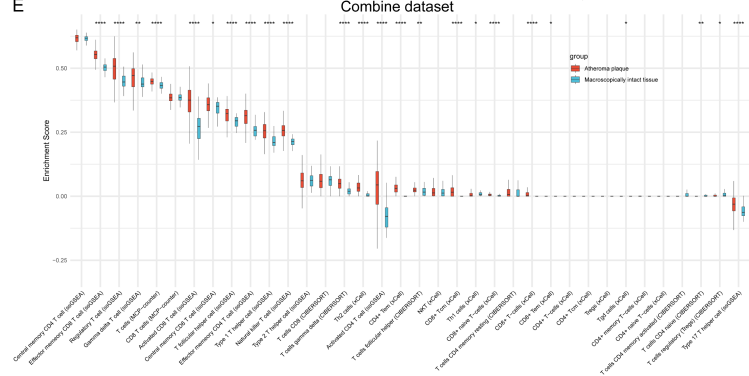
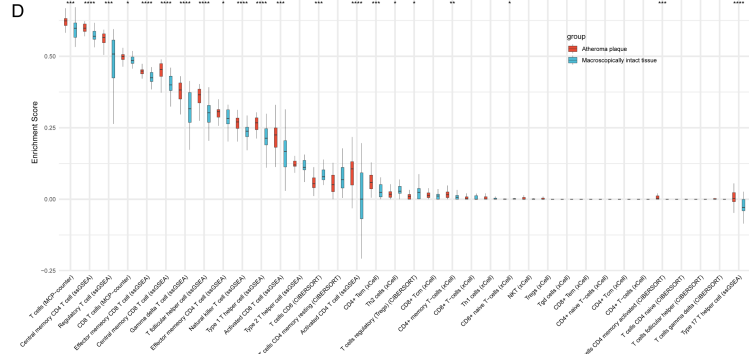
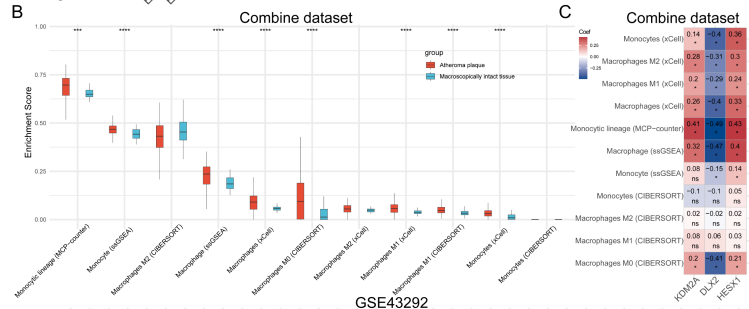
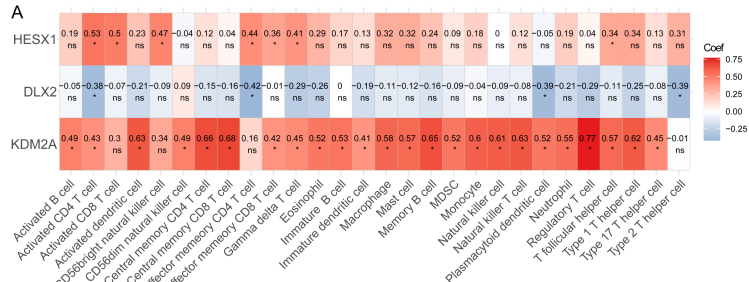
Supplementary figure 8: The KDM2A-FYN axis in peripheral monocytes/macrophages correlates with atherosclerotic severity. The association of (A) KDM2A and (B) FYN expression with carotid plaque severity. (C) Validation of the strong association of KDM2A with RREB1 in GSE56045. The association of RREB1 expression with (D) CAC score and (E) carotid plaque severity. (F) Correlation analysis between KDM2A expression and CpG sites (β values) in 1202 patients. DNA gel electrophoresis showing the relative abundance of (G) Fyn-1 and (H) Fyn-2 promoter fragments among Input, anti-rabbit IgG, and Immunoprecipitation groups. The correlation of the levels of (I) TNF- α , (J) IL-6, and (K) HMGB in serum and Gensini score validated by Enzyme-linked immunosorbent assay (ELISA). Correlation analysis was examined using Pearson's test.

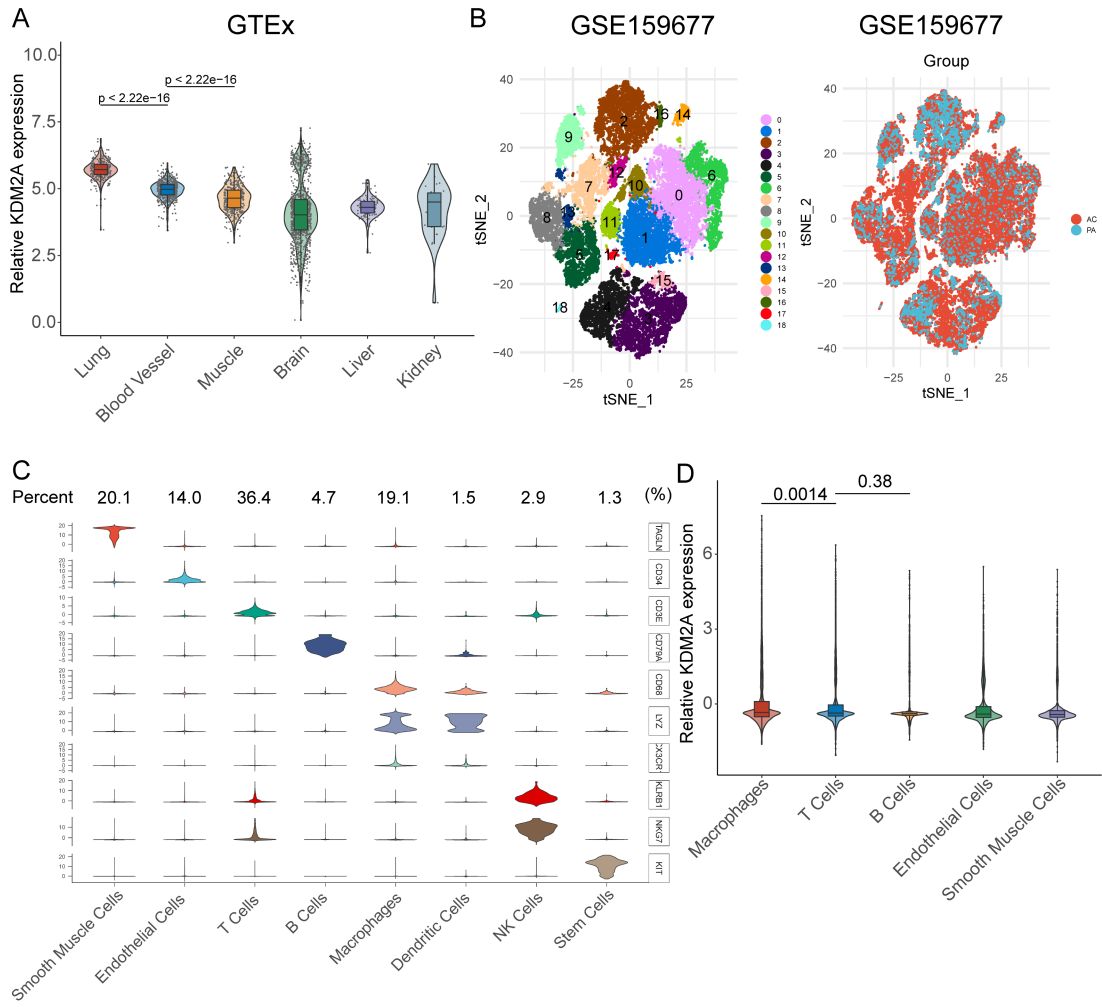
Supplementary figure 9: The experimental flowchart for the AAV9-F4/80-si-KDM2A infection animal experiment.

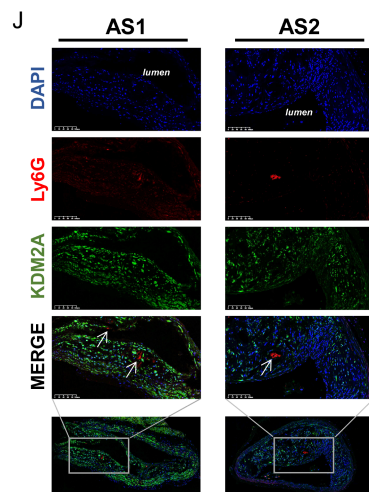
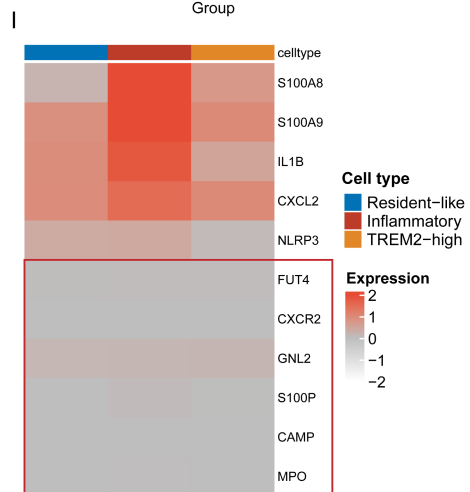
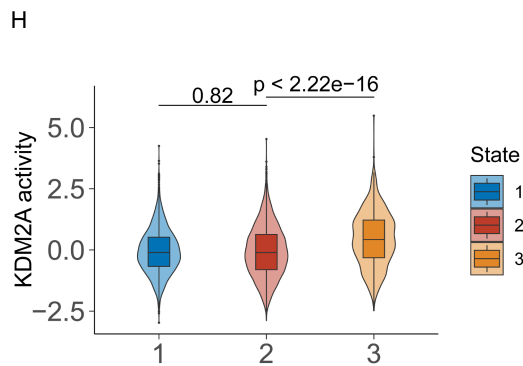
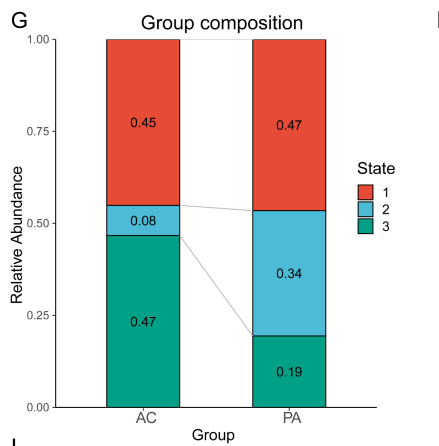
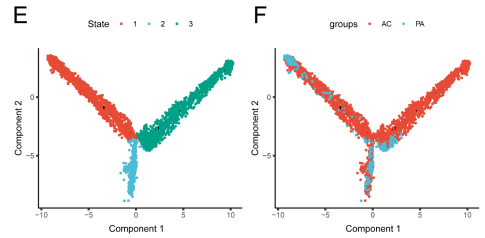
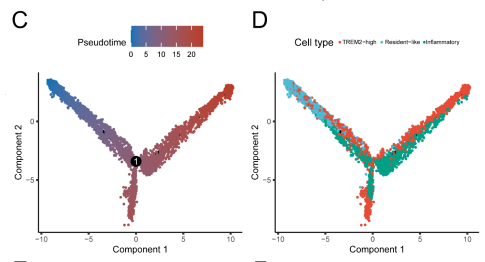
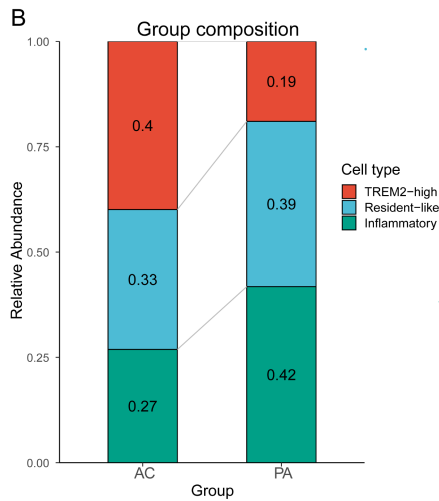
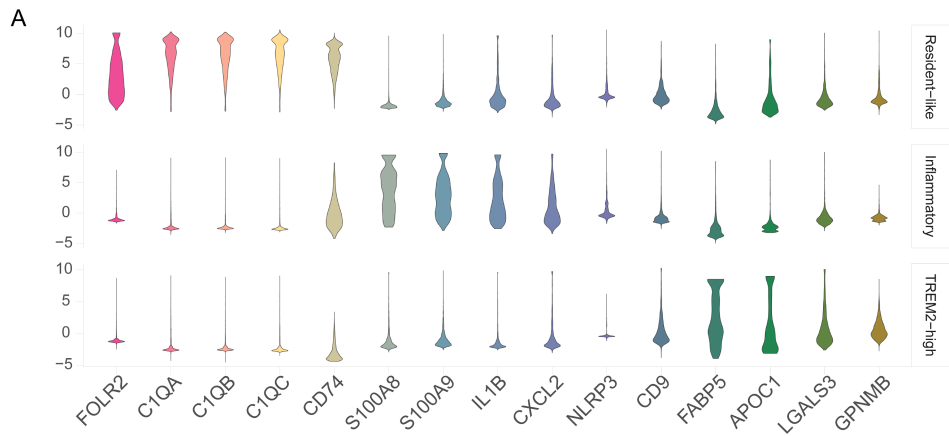
Supplementary figure 10: (A) Representative immunofluorescence analysis of cross-sections of the aortic root stained with KDM2A and CD68. (B) Quantification of the relative intensity KDM2A (B) and percentages of KDM2A⁺ macrophages (CD68⁺ cells) (C). Values are presented as bar plots with group mean \pm SEM. Data were compared by Mann-Whitney U-test.

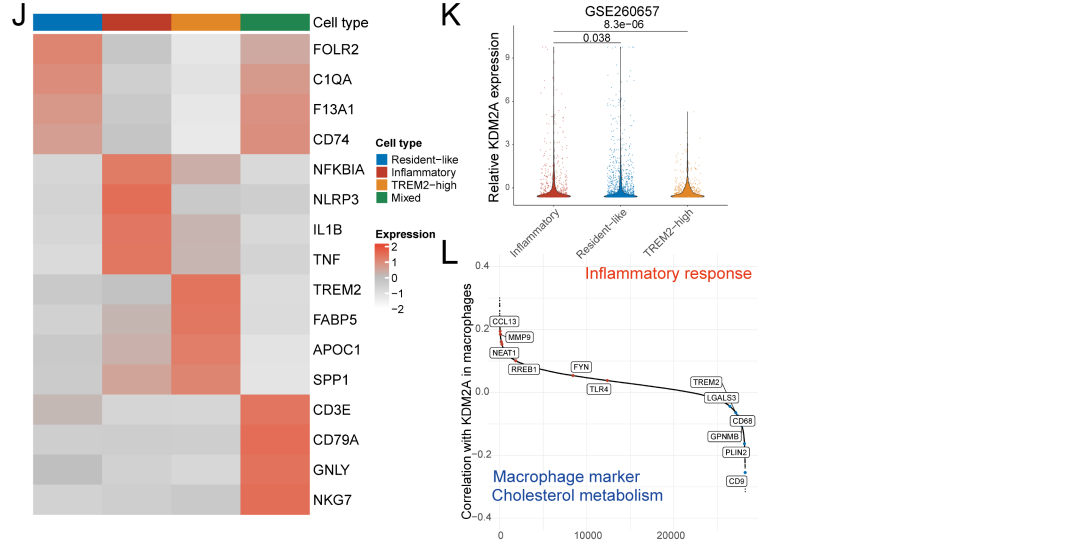
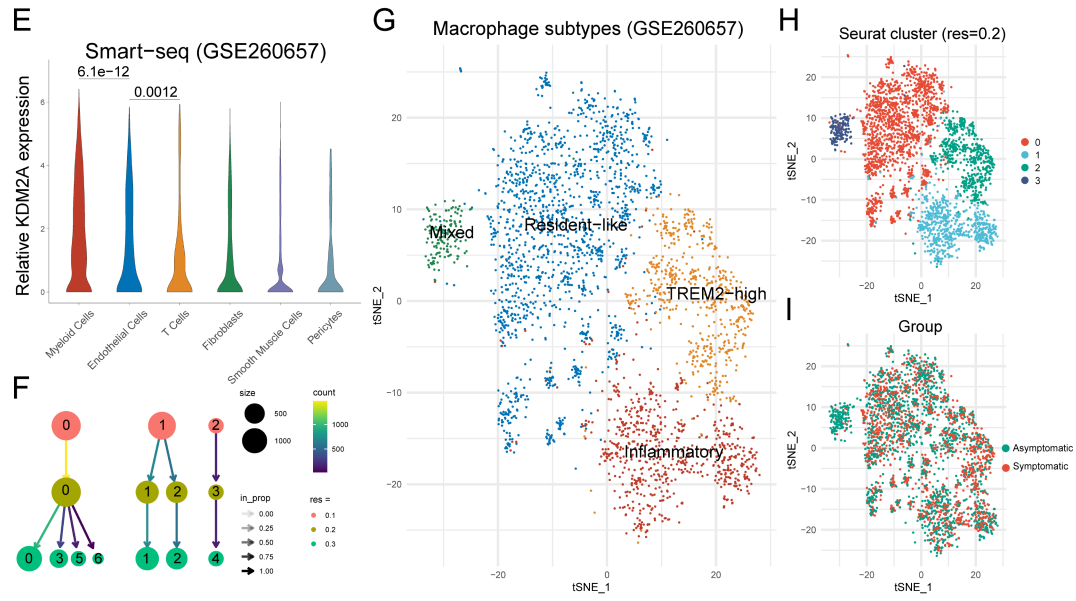
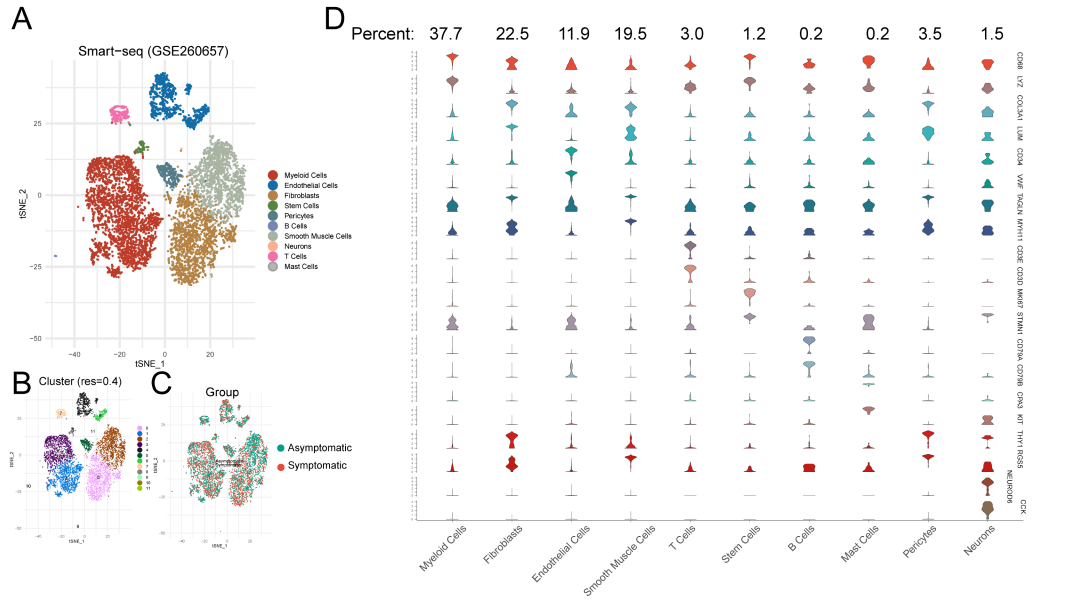
Supplementary figure 11: Causal relationship between KDM2A and atherosclerosis. Leave-one-out plot of the causal relationship between KDM2A and atherosclerosis in (A) UK Biobank and (B) FinnGen database. Surface plot showed the predicted binding models of Kisspeptin-1 (C), NF-449 (D), Colistin (E), Micafungin (F), and TRV-120027 (C) with the Zinc finger of KDM2A.

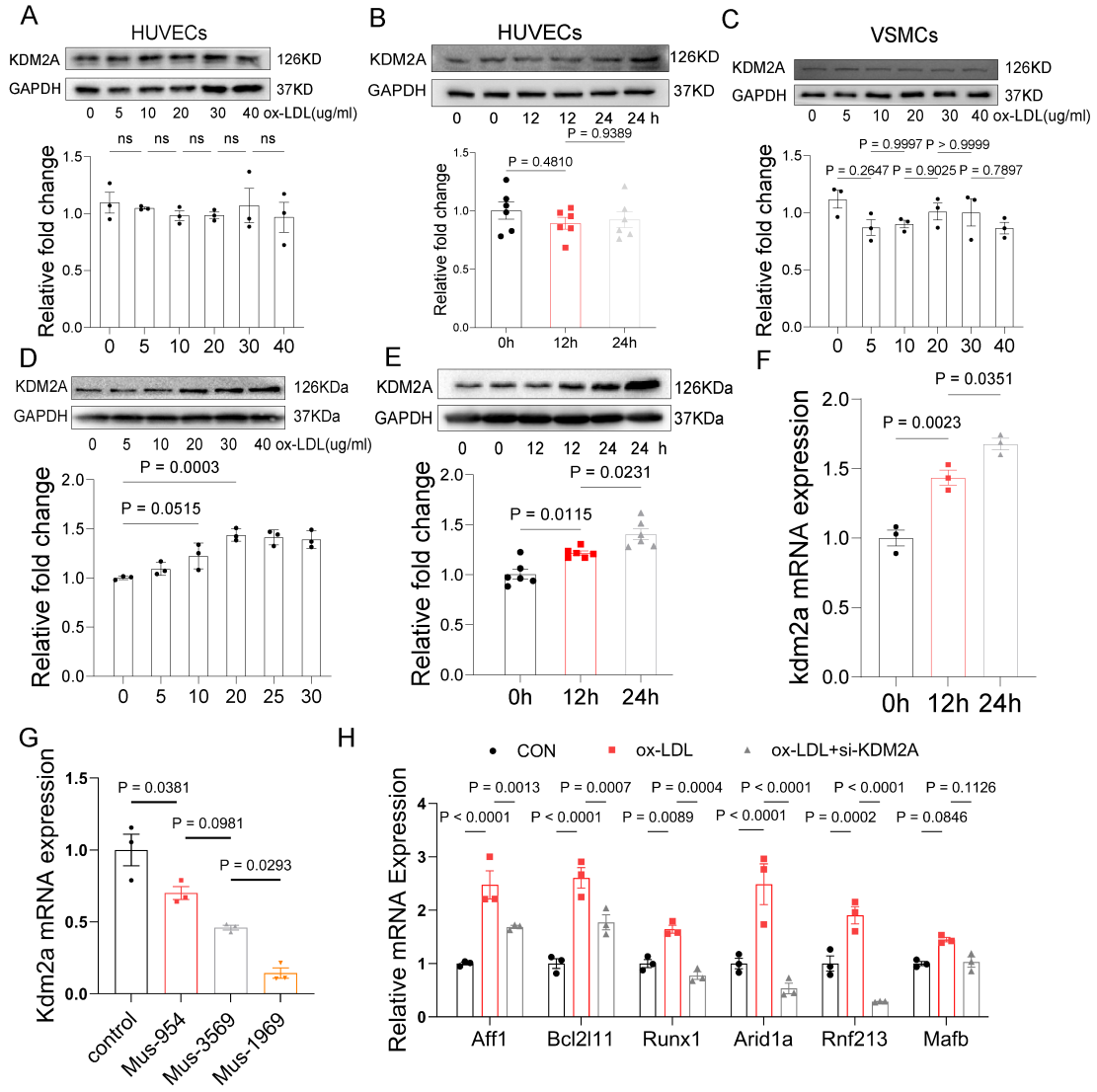


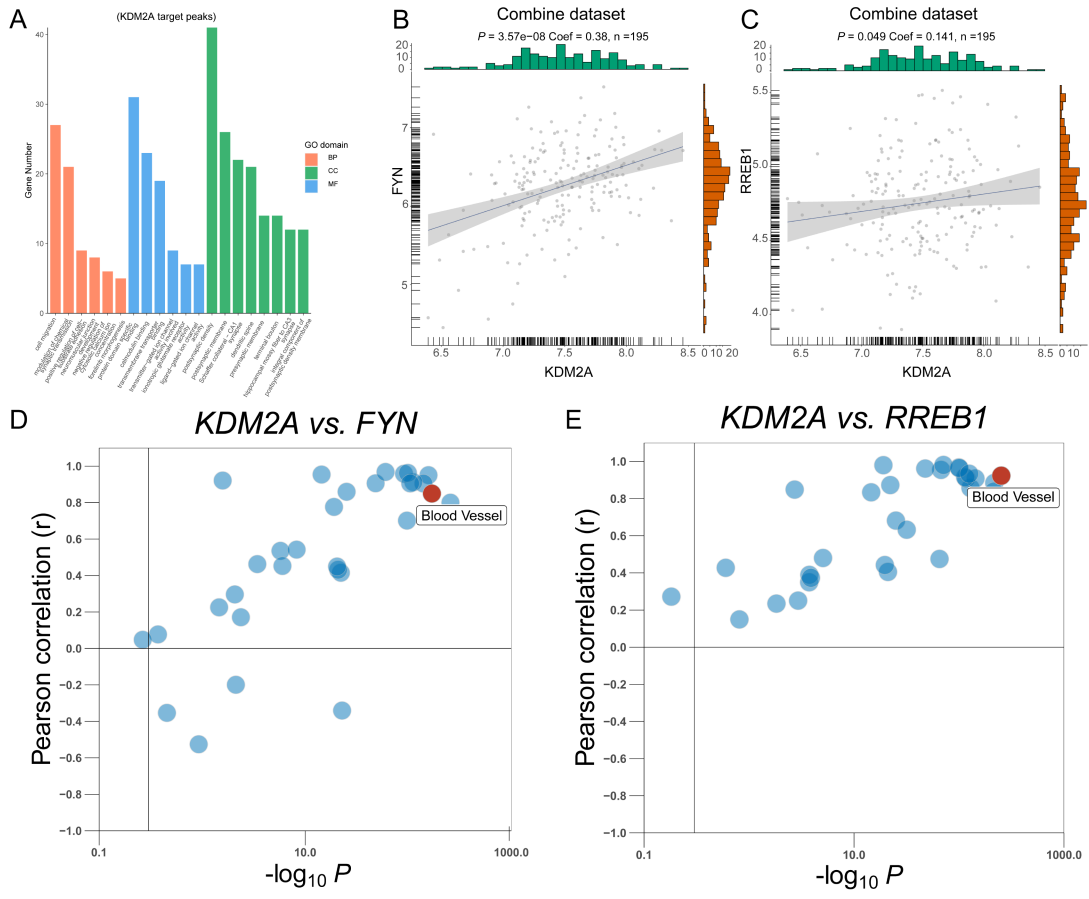


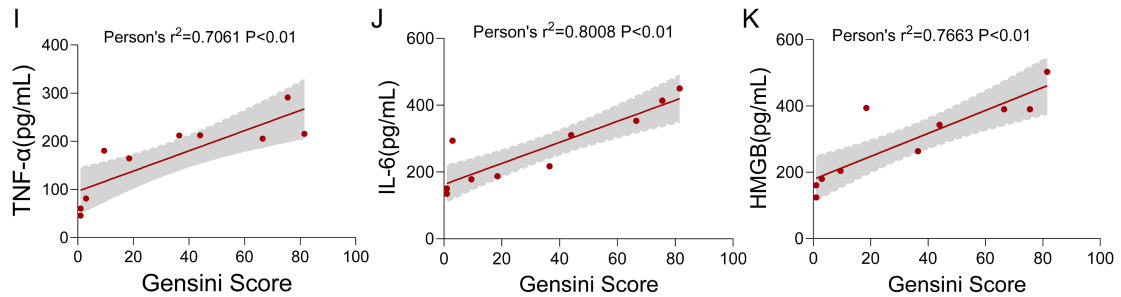
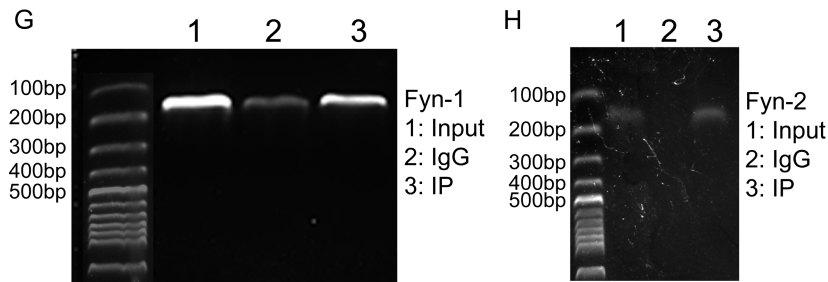
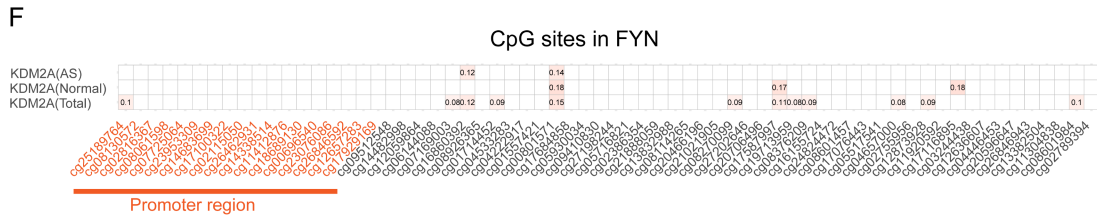
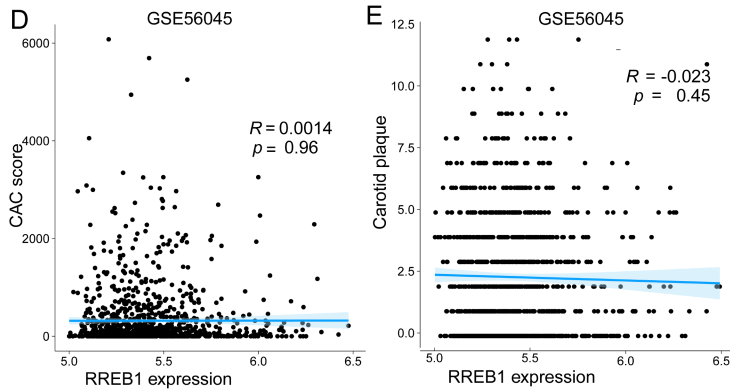
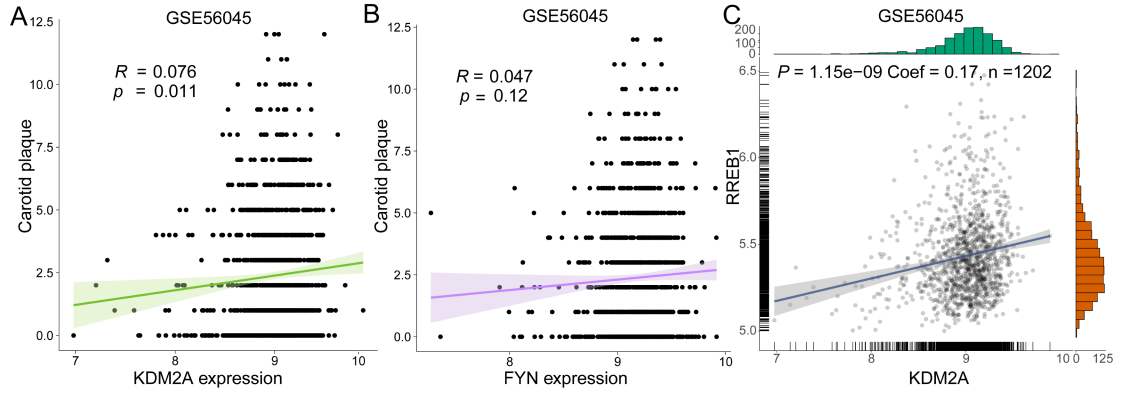


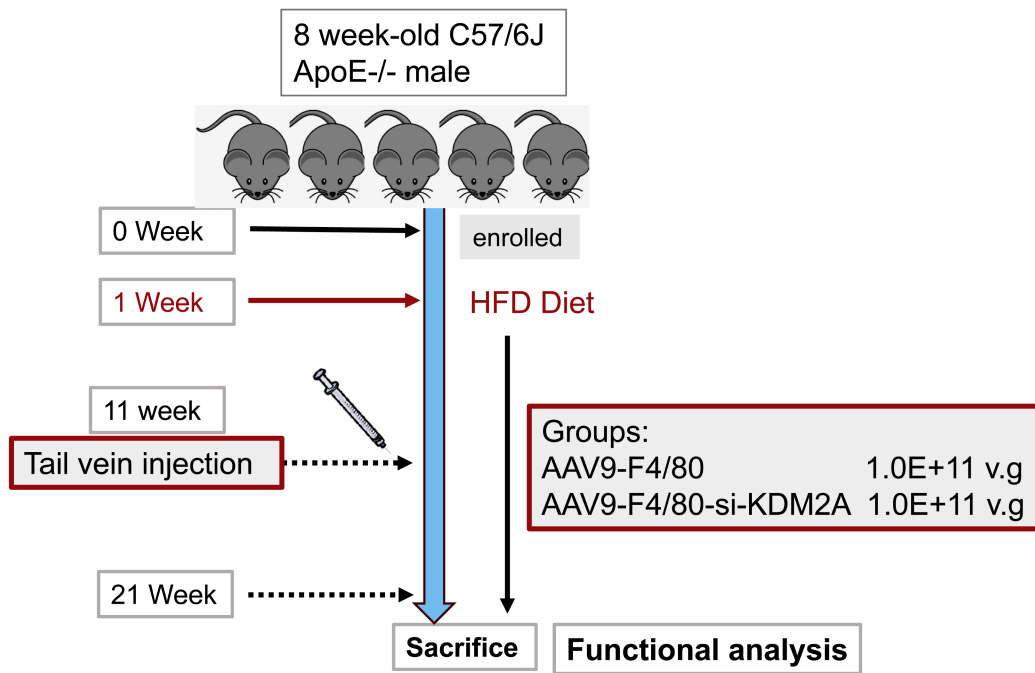


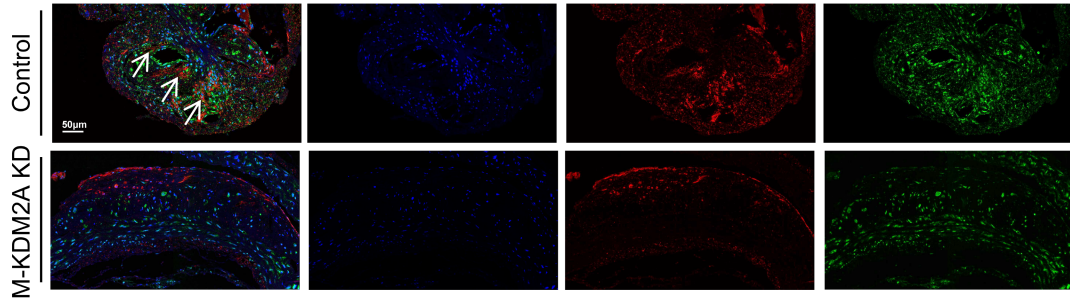
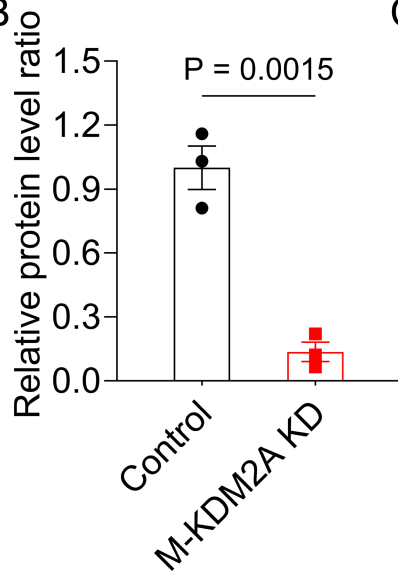










A**CD68/KDM2A/DAPI****B****C**